The Astrophysical Journal Letters, 883:L16 (13pp), 2019 September 20 https://doi.org/10.3847/2041-8213/ab3d30

A Super-Earth and Sub-Neptune Transiting the Late-type M Dwarf LP 791-18

Ian J. M. Crossfield[1], William Waalkes[2,33], Elisabeth R. Newton[3], Norio Narita[4,5,6,7], Philip Muirhead[8], Kristo Ment[9], Elisabeth Matthews[1], Adam Kraus[10], Veselin Kostov[11], Molly R. Kosiarek[12,33], Stephen R. Kane[13], Howard Isaacson[14,15], Sam Halverson[1], Erica Gonzales[16,33], Mark Everett[17], Diana Dragomir[1,34], Karen A. Collins[9], Ashley Chontos[18,33], David Berardo[1,35], Jennifer G. Winters[9], Joshua N. Winn[19], Nicholas J. Scott[20], Barbara Rojas-Ayala[21], Aaron C. Rizzuto[10,36], Erik A. Petigura[22], Merrin Peterson[23], Teo Mocnik[13], Thomas Mikal-Evans[1], Nicholas Mehrle[1], Rachel Matson[20], Masayuki Kuzuhara[4,6], Jonathan Irwin[9], Daniel Huber[18], Chelsea Huang[1], Steve Howell[20], Andrew W. Howard[22], Teruyuki Hirano[24], Benjamin J. Fulton[25], Trent Dupuy[26], Courtney D. Dressing[14], Paul A. Dalba[13,37], David Charbonneau[9], Jennifer Burt[1], Zachory Berta-Thompson[2], Björn Benneke[23], Noriharu Watanabe[6,27], Joseph D. Twicken[20,28], Motohide Tamura[4,6,29], Joshua Schlieder[11], S. Seager[1,30,31], Mark E. Rose[20], George Ricker[1], Elisa Quintana[11], Sébastien Lépine[32], David W. Latham[9], Takayuki Kotani[4,6], Jon M. Jenkins[20], Yasunori Hori[4,6], Knicole Colon[11], and Douglas A. Caldwell[28]

[1] Department of Physics, and Kavli Institute for Astrophysics and Space Research, Massachusetts Institute of Technology, Cambridge, MA, USA; iancross@mit.edu
[2] Department of Astrophysical and Planetary Sciences, University of Colorado, Boulder, CO, USA
[3] Department of Physics and Astronomy, Dartmouth College, Hanover, NH, USA
[4] Astrobiology Center, 2-21-1 Osawa, Mitaka, Tokyo 181-8588, Japan
[5] JST, PRESTO, 2-21-1 Osawa, Mitaka, Tokyo 181-8588, Japan
[6] National Astronomical Observatory of Japan, 2-21-1 Osawa, Mitaka, Tokyo 181-8588, Japan
[7] Instituto de Astrofísica de Canarias (IAC), E-38205 La Laguna, Tenerife, Spain
[8] Department of Astronomy & Institute for Astrophysical Research, Boston University, 725 Commonwealth Avenue, Boston, MA, USA
[9] Center for Astrophysics, Harvard & Smithsonian, 60 Garden Street, Cambridge, MA, USA
[10] Department of Astronomy, University of Texas at Austin, Austin, TX, USA
[11] NASA Goddard Space Flight Center, 8800 Greenbelt Road, MD, USA
[12] Department of Astronomy and Astrophysics, University of California, Santa Cruz, CA, USA
[13] Department of Earth and Planetary Sciences, University of California, Riverside, CA, USA
[14] Astronomy Department, University of California, Berkeley, CA, USA
[15] University of Southern Queensland, Toowoomba, QLD 4350, Australia
[16] Department of Astronomy and Astrophysics, University of California, Santa Cruz, CA 95064, USA
[17] National Optical Astronomy Observatory, Tucson, AZ, USA
[18] Institute for Astronomy, University of Hawai'i, 2680 Woodlawn Drive, Honolulu, HI, USA
[19] Princeton University, Department of Astrophysical Sciences, 4 Ivy Lane, Princeton, NJ, USA
[20] NASA Ames Research Center, Moffett Field, CA, USA
[21] Departamento de Ciencias Fisicas, Universidad Andres Bello, Fernandez Concha 700, Las Condes, Santiago, Chile
[22] Department of Astronomy, California Institute of Technology, Pasadena, CA, USA
[23] Departement de Physique, and Institute for Research on Exoplanets, Universite de Montreal, Montreal, H3T J4, Canada
[24] Department of Earth and Planetary Sciences, Tokyo Institute of Technology, 2-12-1 Ookayama, Meguro-ku, Tokyo 152-8551, Japan
[25] NASA Exoplanet Science Institute, California Institute of Technology, M/S 100-22, 770 S. Wilson Ave, Pasadena, CA, USA
[26] Gemini Observatory, Northern Operations Center, 670 North Aohoku Place, Hilo, HI, USA
[27] Department of Astronomical Science, Graduate University for Advanced Studies (SOKENDAI), Mitaka, Tokyo 181-8588, Japan
[28] SETI Institute, 189 North Bernardo No. 200, Mountain View, CA, USA
[29] Department of Astronomy, University of Tokyo, 7-3-1 Hongo, Bunkyo-ku, Tokyo 113-0033, Japan
[30] Department of Earth, Atmospheric and Planetary Sciences, Massachusetts Institute of Technology, Cambridge, MA, USA
[31] Department of Aeronautics and Astronautics, MIT, 77 Massachusetts Avenue, Cambridge, MA, USA
[32] Department of Physics and Astronomy, Georgia State University, GA, USA

Received 2019 June 21; revised 2019 August 19; accepted 2019 August 20; published 2019 September 19

Abstract

Planets occur most frequently around cool dwarfs, but only a handful of specific examples are known to orbit the latest-type M stars. Using *TESS* photometry, we report the discovery of two planets transiting the low-mass star called LP 791-18 (identified by *TESS* as TOI 736). This star has spectral type M6V, effective temperature 2960 K, and radius 0.17 $R_\odot$, making it the third-coolest star known to host planets. The two planets straddle the radius gap seen for smaller exoplanets; they include a 1.1$R_\oplus$ planet on a 0.95 day orbit and a 2.3$R_\oplus$ planet on a 5 day orbit. Because the host star is small the decrease in light during these planets' transits is fairly large (0.4% and 1.7%). This has allowed us to detect both planets' transits from ground-based photometry, refining their radii and orbital ephemerides. In the future, radial

[33] NSF Graduate Research Fellow.
[34] NASA Hubble Fellow.
[35] NSERC Graduate Research Fellow.
[36] 51 Pegasi b Fellow.
[37] NSF Astronomy and Astrophysics Postdoctoral Fellow.

velocity observations and transmission spectroscopy can both probe these planets' bulk interior and atmospheric compositions, and additional photometric monitoring would be sensitive to even smaller transiting planets.

Unified Astronomy Thesaurus concepts: Exoplanet astronomy (486); Exoplanet systems (484); High resolution spectroscopy (2096); Low mass stars (2050); Transit photometry (1709)

1. Introduction

Cool, low-mass stars—M dwarfs—are more numerous and host more short-period planets per star than the more massive stars that host most of the known planets (Bonfils et al. 2013; Dressing & Charbonneau 2015; Mulders et al. 2015). Whether they are seen to transit, inferred from radial velocity spectroscopy or detected via gravitational microlensing, exoplanets tend to be easier to characterize when they orbit M dwarfs instead of larger, hotter, more massive stars. These red dwarfs are therefore popular targets for exoplanet surveys of all types.

The *Kepler* mission surveyed several thousand M dwarfs for transiting exoplanets and revealed that planet occurrence rates increase with decreasing stellar mass and $T_{\rm eff}$ for $P < 1$ yr (Howard et al. 2012). However, most of *Kepler*'s M dwarfs were early-type: fewer than 600 had $T_{\rm eff} < 3300$ K (Dressing & Charbonneau 2013; Morton & Swift 2014; Hardegree-Ullman et al. 2019) and would therefore be in the regime of stars with fully convective interiors. Just seven stars that are cooler than $T_{\rm eff} < 3100$ K are known to host planets.[38] The coolest of these is TRAPPIST-1 ($T_{\rm eff} \approx 2600$ K, 0.08 $M_{\odot}$; Gillon et al. 2017), whose seven transiting planets hint that the number of planets per star may be high for the lowest-mass stars and have sparked a flurry of theoretical and observational follow-up studies.

It remains an outstanding question as to whether planet occurrence continues to increase toward the lowest stellar masses (or beyond: do brown dwarfs host planets?), and how these planets compare to those orbiting hotter stars. Although not a statistical mission, the *TESS* nearly all-sky transit survey (Ricker et al. 2014) can help to answer this question. *TESS* will survey 70% of the sky over its two year prime mission, and is therefore well positioned to aid the search for planets around nearby M dwarfs. Compared to *Kepler*, a much larger percentage of the *TESS* project's high-priority target list consists of M dwarfs, including some of the latest-type M dwarfs. One of the first planets discovered by *TESS*, LHS 3844b (Vanderspek et al. 2019), orbits an M5V star and is consequently proving to be an excellent target for detailed characterization.

We report here the statistical validation of two exoplanets orbiting LP 791-18 (2MASS J11024596-1624222, TIC 181804752), which was recently observed by *TESS*. At $T_{\rm eff} =$ 2960 K this is the third-coolest star known to host exoplanets. Thus, like TRAPPIST-1 (Gillon et al. 2017), GJ 1214 (Charbonneau et al. 2009), Proxima Centauri (Anglada-Escudé et al. 2016), and other similar systems, it represents another rare laboratory to study exoplanets around the very smallest stars.

2. Observations

Our target was first identified as a star of more than average interest by Luyten (1979), who noted its high proper motion and red color as part of the Luyten Palomar survey. Therefore, we henceforth refer to the star as LP 791-18. The star's properties were more recently estimated in the *TESS* Cool Dwarf Catalog (Muirhead et al. 2018). It was found to be an attractive target for *TESS* transit photometry, and was scheduled for observations at a two-minute cadence during Sector 9 of the *TESS* prime mission on account of its inclusion on the high-priority *TESS* Candidate Target List (Stassun et al. 2018b) and as part of *TESS* Guest Investigator program GO 11180 (PI: Dressing). We note that all data products used in the succeeding sections have been made available to the community on the ExoFOP-TESS website.[39] A summary of all relevant stellar and planet properties are given in Tables 1 and 2, respectively.

2.1. TESS *Transit Photometry*

TESS observed LP 791-18 nearly continuously from 2019 March 1 to 25 at a two-minute ("short") cadence. Initial data processing was similar to that of π Men (Huang et al. 2018), LHS 3844b (Vanderspek et al. 2019), and other recent *TESS* discoveries. Analysis by the *TESS* Science Processing Operations Center (Jenkins 2002; Jenkins et al. 2016) identified two possible planetary signals, and human vetting of the data reports (Twicken et al. 2018; N. Guerrero et al. 2019, in preparation; Li et al. 2019) resulted in the announcement of planet candidates TOI-736.01 and .02. The *TESS* Pre-Search Data Conditioning Simple Aperture Photometry (PDC_SAP) light curve (Smith et al. 2012; Stumpe et al. 2014) is shown in Figure 1. Individual transits of the larger, longer-period TOI-736.01 are visible by eye, while the shallower, shorter-period TOI-736.02 can only be seen in the phase-folded photometry. These two signals have Multiple Event Statistics of 17.7 and 7.7, respectively. As a semi-independent check we also used the *TESS* Quick-Look Pipeline (C. Huang et al. 2019, in preparation) to confirm that the transit-like events are visible in the *TESS* long-cadence data, but the short transit durations make those data unsuitable for a detailed light-curve analysis.

We used the short-cadence light curve to conduct a transit analysis of both signals, using the same software as described by Crossfield et al. (2016, 2017). The only difference from those analyses of long-cadence *K*2 photometry is that we now numerically integrate each model light curve over just the two-minute (not 30 minute) duration of each point. As in those analyses, we impose priors on the quadratic limb-darkening coefficients. Based on the stellar parameters derived below and the distribution of coefficients from Claret (2018), we adopted Gaussian priors of $u_1 = 0.26 \pm 0.06$ and $u_2 = 0.55 \pm 0.07$. Our best-fit transit models for both signals are shown in Figure 1, and the model parameters are listed in Table 2. The best-fit mid-transit times (in $\rm BJD_{TDB}$) from the *TESS* photometry are $T_0 =$ 2458546.50885 $\pm$ 0.00096 and 2458543.5584 $\pm$ 0.0017 for TOI-736.01 and .02, respectively.

We performed an independent check on our light curve analysis, using an approach similar to that described by Chontos et al. (2019). This parameterization fits for P, T_0, quadratic limb-darkening coefficients (u_1, u_2), $\rho_{*,\rm circ}$, b, R_P/R_*, and a photometric normalization. Again, we assume a linear ephemeris, circular orbit, and quadratic limb-darkening law with Gaussian priors imposed. Additional priors were used to constrain u_1 to the interval [0, 2], u_2 to [−1, 1], and to ensure $\rho_{*,\rm circ} > 0$. We explored the parameter space using the `emcee` Markov chain Monte Carlo algorithm (Foreman-Mackey et al. 2013), initializing

[38] According to the NASA Exoplanet Archive, 2019 June.

[39] https://exofop.ipac.caltech.edu/tess/target.php?id=181804752

Table 1
Stellar Parameters of LP 791-18

Parameter	Value	Source
Identifying Information		
TIC ID	181804752	TIC v8 (Stassun et al. 2018a)
α R.A. (hh:mm:ss)	11:02:45.96	
δ Decl. (dd:mm:ss)	−16:24:22.29	
μ_α (mas yr^{-1})	−221.08 ± 0.22	*Gaia* second data release (DR2)
μ_δ (mas yr^{-1})	−59.00 ± 0.14	*Gaia* DR2
Distance (pc)	26.493 ± 0.064	*Gaia* DR2 (Bailer-Jones et al. 2018)
Photometric Properties		
V (mag)	16.9 ± 0.2	TIC v8
G (mag)	15.0715 ± 0.0013	*Gaia* DR2 (Gaia Collaboration et al. 2018)
G_{BP} (mag)	17.23831 ± 0.0072	*Gaia* DR2
G_{RP} (mag)	13.69512 ± 0.0029	*Gaia* DR2
u (mag)	21.28 ± 0.14	Sloan Digital Sky Survey (SDSS; Albareti et al. 2017)
g (mag)	17.8827 ± 0.0057	SDSS
r (mag)	16.2672 ± 0.0039	SDSS
i (mag)	14.3142 ± 0.0035	SDSS
z (mag)	13.2565 ± 0.0035	SDSS
J (mag)	11.559 ± 0.024	Two Micron All-Sky Survey (2MASS; Skrutskie et al. 2006)
H (mag)	10.993 ± 0.022	2MASS
Ks (mag)	10.644 ± 0.023	2MASS
$W1$ (mag)	10.426 ± 0.023	AllWISE (Cutri et al. 2012)
$W2$ (mag)	10.233 ± 0.021	AllWISE
$W3$ (mag)	10.024 ± 0.062	AllWISE
Spectroscopic and Derived Properties		
Spectral Type	M(6.1 ± 0.7)V	This work
Barycentric rv (km s^{-1})	+14.1 ± 0.3	This work
Age (Gyr)	>0.5	This work
[Fe/H]	−0.09 ± 0.19	This work
$T_{\rm eff}$ (K)	2960 ± 55	This work
$\log_{10} g$ (cgs)	5.115 ± 0.094	This work
$v \sin i$ (km s^{-1})	<2	This work
M_* ($M_\odot$)	0.139 ± 0.005	This work
R_* ($R_\odot$)	0.171 ± 0.018	This work
L_* ($L_\odot$)	0.00201 ± 0.00045	This work

100 walkers and having each take 20,000 steps. A burn-in phase of 5000 steps was removed before compiling the final posterior distribution for each parameter. Our two transit analyses are consistent, agreeing to within 1σ for all of the derived quantities.

Following the methodology of Berardo et al. (2019), we also conducted a search for transit timing variations (TTVs) by fitting each transit of TOI-736.01 individually, allowing only the transit midpoints to vary. By comparing these individual times to a linear ephemeris, we conclude that there are no significant TTVs for either of the signals.

We also examined the TESS light curve for stellar flares, but found none. We estimate that we would have easily detected any flares that were $\gtrsim$3% of the stellar luminosity in the TESS bandpass. However, this is a very loose constraint that corresponds (for flare durations >4 minutes) to flare energies of $>5 \times 10^{31}$ erg—much stronger than the typical flare energies for such stars (Ilin et al. 2019; Paudel et al. 2019) and 10 times fainter than the strongest flare observed from TRAPPIST-1 (Paudel et al. 2019). More precise photometry would be needed to say whether moderate-intensity flares are common on this star, but the lack of such strong superflares indicates that LP 791-18 is not a particularly active star.

2.2. Stellar Properties from Archival Photometry

We estimate the spectral type of LP 791-18by comparing the *Gaia* DR2 photometry and parallax (Gaia Collaboration et al. 2018) to color-type and absolute magnitude-type relations (Kiman et al. 2019). The six possible relations indicate an M dwarf with subclass mean and standard deviation of 6.1 ± 0.7, which we adopt as the spectral type of our target. LP 791-18 is not elevated above the main sequence when plotted on an optical-infrared color–magnitude diagram, indicating that the star is not an unresolved near-equal-mass binary—unless it has a markedly sub-solar metallicity, which we rule out below.

We estimate the stellar mass using the K_S-band mass–luminosity relation of Mann et al. (2019). The statistical and systematic uncertainties on the derived mass are both 0.0033 $M_\odot$, so we report $M_* = 0.139 \pm 0.005$. This mass is consistent with that derived from earlier V- and K-band mass–luminosity relations (Benedict et al. 2016).

We estimate the stellar radius using the absolute magnitude versus radius relations of Mann et al. (2015). Those authors indicate that the JHK_S relations are their most precise. Taking the weighted mean of the three derived radii, we find $R_* = 0.171 \pm 0.018$. This radius and the mass are consistent with the mass–radius relation for low-mass stars (Mann et al. 2015).

We estimate the stellar effective temperature using calibrated photometric color relations. Mann et al. (2015) demonstrated a tight correlation between $T_{\rm eff}$ and $(V - J)$, $(r - z)$, and $(r - J)$. These relations all have intrinsic scatters of about 55 K, so we take the mean of the three derived temperatures to find $T_{\rm eff} = 2960 \pm 55$ K. This value is consistent with temperatures estimated from tabulated photometric relations and from our derived spectral type (Kraus & Hillenbrand 2007; Pecaut & Mamajek 2013).

We estimate the stellar metallicity using photometric relations. The approach of Schlaufman & Laughlin (2010) gives the best agreement with near-infrared spectroscopic metallicities (Rojas-Ayala et al. 2012). Using their methodology, we find $\Delta(V - K_S) = 0.2$, which implies [Fe/H] $= -0.02 \pm 0.21$ (accounting for the relation's intrinsic scatter and our uncertainty on V). Comparison to the $(G_R - J)$, M_K color–magnitude diagram of Kesseli et al. (2019) indicates a consistent metallicity of -0.5 ± 0.5. We report the weighted mean of these two independent estimates, [Fe/H] $= -0.09 \pm 0.19$.

As previously noted, LP 791-18's properties were also estimated by Muirhead et al. (2018) using broadband photometry but without the benefit of *Gaia* DR2. All of their stellar parameters are within 1σ of ours, as can be seen by comparing Table 1 with the values reported in that work.

2.3. High-resolution Spectroscopy

To further characterize the system and check for any evidence of spectroscopic binaries that could indicate a non-planetary origin for the transit signals, we obtained high-resolution spectra from the Keck/High Resolution Echelle

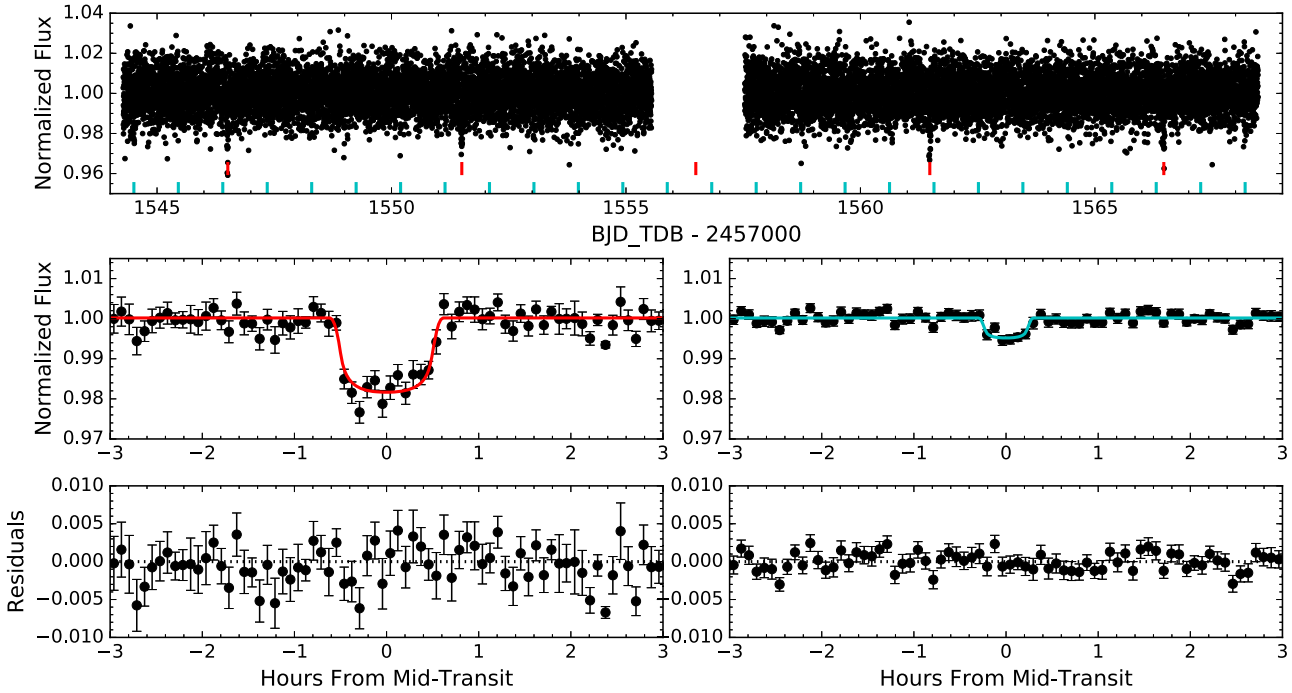

Figure 1. Top panel: *TESS* short-cadence photometry of LP 791-18. Vertical ticks indicate the locations of each planets' transits. Middle panels: phase-folded photometry (binned to five-minute intervals, with errorbars indicating the standard error on the mean in each bin) and best-fit light curves for each planet. Bottom panels: residuals to the transit fits.

Table 2
Planet Parameters

Parameter	Units	LP 791-18b (TOI-736.02)	LP 791-18c (TOI-736.01)
T_0	$BJD_{\rm TDB} - 2457000$	1645.94405 ± 0.00066	1651.29807 ± 0.00041
P	day	0.9480050 ± 0.0000058	4.989963 ± 0.000050
i	deg	$87.3^{+2.0}_{-4.9}$	$89.55^{+0.32}_{-0.50}$
R_P/R_*	...	0.0604 ± 0.0028	0.1238 ± 0.0022
R_*/a	...	$0.090^{+0.058}_{-0.016}$	$0.0290^{+0.0035}_{-0.0016}$
T_{14}	hr	$0.612^{+0.068}_{-0.079}$	$1.208^{+0.056}_{-0.046}$
T_{23}	hr	$0.466^{+0.076}_{-0.259}$	$0.899^{+0.041}_{-0.048}$
b	...	$0.54^{+0.36}_{-0.37}$	$0.28^{+0.24}_{-0.19}$
$\rho_{*,\rm circ}$	g cm^{-3}	28 ± 22	$31.1^{+5.6}_{-9.1}$
a	au	$0.00969^{+0.00032}_{-0.00035}$	$0.029392^{+0.00098}_{-0.00105}$
R_P	$R_{\rm E}$	1.12 ± 0.13	2.31 ± 0.25
$S_{\rm inc}$	$S_{\rm E}$	$21.5^{+5.4}_{-4.6}$	$2.35^{+0.59}_{-0.51}$
$T_{\rm eq}$[a]	K	650 ± 120	370 ± 30

Note.
[a] Assuming a uniform random distribution of Bond albedos (0–0.4) and heat redistribution factors (0.25–0.5).

Spectrometer (HIRES) and Subaru/InfraRed Doppler (IRD) instruments.

2.3.1. Keck/HIRES

We acquired an optical spectrum using Keck/HIRES (Vogt et al. 1994) on 2019 June 12. The observation took place in 1.″0 effective seeing and using the C2 decker without the iodine gas cell, giving an effective resolution of $\lambda/\Delta\lambda \approx 55{,}000$. We exposed for 1386 s and obtained signal-to-noise ratio (S/N) of roughly 30 per pixel. Data reduction followed the standard approach of the California Planet Search consortium (Howard et al. 2010).

Using the approach of Kolbl et al. (2015), we examined our spectrum for secondary components that would indicate the presence of another star. We found no evidence of additional lines down to the method's standard sensitivity limit of $\Delta V = 5$ mag for $\Delta v > 10$ km s^{-1}, consistent with LP 791-18 being a single, isolated star. Finally, we measured LP 791-18's absolute radial velocity following Chubak et al. (2012), finding 14.1 ± 0.1 km s^{-1}.

We compare our HIRES spectrum with several archival spectra of other cool M dwarfs (Figure 2). LP 791-18's spectrum is very similar to an archival HIRES spectrum of the M5V GJ 1214 (suggesting generally similar metallicity and temperature), but with slightly broader K I line (consistent with

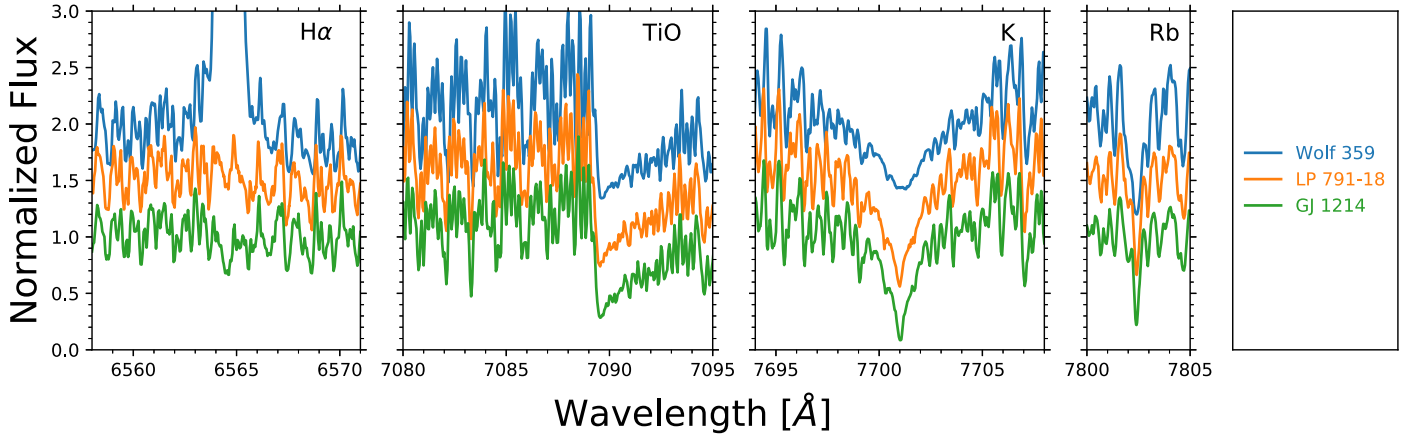

Figure 2. Comparison of Keck/HIRES spectra of LP 791-18 (orange) with GJ 1214 (green) and Wolf 359 (blue) in the vicinity of the expected locations of Hα, TiO bands, K I (7701.0 Å), and Rb I (7802.4 Å). No secondary spectral lines are detected.

higher surface gravity). Aside from this pressure-broadened line, the widths of weaker lines in these two stars are indistinguishable, consistent with a low projected rotational velocity for both stars ($v \sin i < 2$ km s^{-1} for GJ 1214; Charbonneau et al. 2009). In comparison, LP 791-18's lines are noticeably narrower than those seen in archival HIRES spectra of the M6V Wolf 359, which has $v \sin i < 3$ km s^{-1} (Jenkins et al. 2009). However, we note that if LP 791-18 is typical of old, low-mass M dwarfs and has a rotation period of roughly 100 days (Newton et al. 2017), then $v \sin i \sim 0.1$ km s^{-1}. The lack of Hα emission (see Figure 2) in a star of this mass also indicates that the star likely has a rotation period >100 days (Newton et al. 2017). Thus, the value reported in Table 1 of $v \sin i < 2$ km s^{-1} should be taken as a conservative upper limit.

Several additional lines of evidence are consistent with this interpretation of LP 791-18 as a relatively old star. First, we do not detect the Li line, indicating that LP 791-18 is older than 0.5 Gyr (Reiners & Basri 2009). Second, Hα is not seen in emission (see Figure 2); though there is no true continuum against which to compare the line, Hα appears to be slightly in absorption (with a similar depth and profile to GJ 1214), suggesting a long rotation period (as noted above) and therefore an age of several Gyr (Newton et al. 2016). Furthermore, comparison of our inferred M_*, R_*, and L_* to evolutionary models of ultracool dwarfs (Fernandes et al. 2019) also indicates an age $\gtrsim$0.4 Gyr. In addition, the Galactic space velocity of LP 791-18 is not consistent with any of the known young moving groups or associations (Gagné et al. 2018), with a 95.7% likelihood of it being a field star (according to `BANYAN-SIGMA`; Gagné et al. 2018); its dynamics are consistent with the thin disk rather than with the thick disk or halo. All these points, combined with the lack of large-amplitude variations or flares in *TESS* or MEarth photometry (Newton et al. 2018) suggest that LP 791-18 has an age $\gtrsim$0.5 Gyr, and likely at least several Gyr.

2.3.2. Subaru/IRD

We observed LP 791-18 with the IRD (Kotani et al. 2018) behind an adaptive optics (AO) system (AO188; Hayano et al. 2010) on the Subaru 8.2 m telescope on 2019 June 17. We took three spectra with exposure times of 600 s each, with airmass of 1.8–2.0, covering the wavelength range from 0.95 to 1.76 μm at spectral resolution ≈70,000. We processed the spectra using standard tools that are based on Python and PyRAF. The tools perform bias subtraction, flat-fielding, scattered light subtraction, correction of pixels with irregularly high counts, order tracing, and spectral extraction. An absolute wavelength solution was assigned using Th–Ar calibration spectra (Kerber et al. 2008) and laser frequency comb spectra, both of which were taken during daytime observations in the 2019 June observing run.

We combined our three exposures into one template spectrum for visual inspection of possible contamination of any additional faint stars. Achieved S/N around the peaks of blaze function in the combined spectrum is roughly 30 in *Y*, 50 in *J*, and 80 in *H*. Figure 3 shows the combined spectrum of LP 791-18 along with a rapidly rotating star HR 4064, taken immediately after the exposures for LP 791-18, with airmass of 2.1. As with our HIRES analysis, we do not see any evidence of contaminating lines in the spectrum.

2.4. High-resolution Imaging

TESS has large pixels (21″ across), which are large enough to contain many additional stars that could potentially be the source of the detected transits. To identify any additional stars around LP 791-18, we obtained several sets of high-resolution imaging data, as described below.

2.4.1. Gemini/'Alopeke Optical Speckle Imaging

We observed LP 791-18 with the 'Alopeke speckle imaging instrument (Howell et al. 2011; Scott & Howell 2018) on the Gemini-North 8.1 m telescope on 2019/06/08. The observations consisted of 18 simultaneous image sets of one thousand 60 ms frames in narrow band filters centered at 562 and 832 nm in good observing conditions, with the native seeing measured to be 0.″4. Because our target is quite red, the data at 832 nm are superior to those at 562 nm. The speckle images were reduced alongside the point source calibrator star HR 4284 standard reduction procedures (Howell et al. 2011; Matson et al. 2018). Data products include the power spectrum of the speckle patterns of LP 791-18 divided by those of HR 4284, and a reconstructed image of the 2.″5 × 2.″5 field centered on the target (shown in Figure 4).

These data products were inspected for neighboring sources and none were found. Contrast curves were produced from the reconstructed images by normalizing the peak flux of the star and determining the standard deviation in magnitudes among

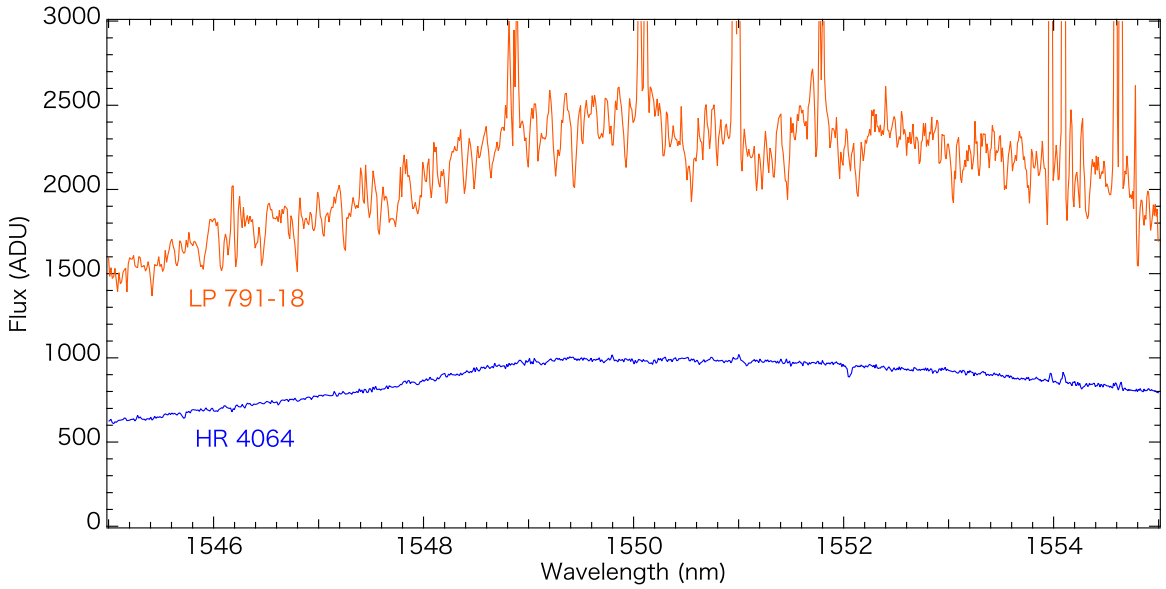

Figure 3. Subaru/IRD spectrum of LP 791-18 (orange) and the rapidly rotating star HR 4064 (blue). The vertical axis represents fluxes in digital units (the detector gain is 2.78 e^- per digital unit). The flux of HR 4064 has been decreased by a factor of 10 for plotting purposes. The apparent emission lines seen in the spectrum of LP 791-18 are due to telluric airglow. Again, no secondary lines are seen in the spectrum of LP 791-18.

local minima and maxima in the background noise as a function of angular separation from the star. A flux level 5σ brighter than the mean of the local extrema is used to define the limiting contrast relative to the LP 791-18. At 832 nm we achieve a contrast of 4.8 mag at $0\farcs1$, increasing steadily to 7.0 mag at $1\farcs2$, as shown in Figure 4.

2.4.2. Keck/NIRC2 AO Imaging and Aperture Masking

On 2019 June 12 we obtained laser guide star adaptive optics (LGS-AO) imaging (Wizinowich et al. 2000) and non-redundant aperture masking interferometry (NRM; Tuthill et al. 2006) of LP 791-18 in two visits separated by 15 minutes with Keck/NIRC2. The observations were taken in vertical angle mode without dithering and using the K' filter, and the NRM used the nine-hole mask. We also observed two nearby calibrator stars. In all cases we used the smallest pixel scale of 9.952 mas pix^{-1}. For imaging we took 12 exposures, each with 20 coadds of 1 s duration and four Fowler samples. For NRM we took 16 interferograms, each with one coadd lasting 20 s and comprising 64 Fowler samples. For the first calibrator we obtained eight images and eight interferograms in similar setups. For the second calibrator we obtained eight images and four interferograms.

On 2019 June 13 we obtained additional LGS-AO imaging of LP 791-18 and the first calibrator star, again in K' at the same pixel scale. The observations were taken in position angle mode, rotated to align the $+y$ axis of NIRC2 with North. We observed in a three-point dither pattern that avoided the NIRC2 bad quadrant while stepping the target in offsets of $1\farcs0$, $1\farcs5$, and $2\farcs0$; we did not dither on the calibrator. We took 20 exposures of LP 791-18 using the same settings as in the preceding night, and took eight exposures of the first calibrator.

We reduced each frame and searched the resulting data for companions following Kraus et al. (2016). We used two different strategies for point-spread function (PSF) subtraction, applied individually to each image. To search for faint, wide companions at >500 mas, we subtracted a model constructed from the azimuthally averaged flux profile of LP 791-18. This added no additional noise at wide separations, but left the speckles in place, making it non-ideal for detecting close-in companions. To probe smaller inner working angles we then also subtracted a scaled version of the best-fitting empirical PSF taken from the set of all imaging observations of the calibrator stars. We measured the flux as a function of position within each residual image using 40 mas (radius) apertures centered on every image pixel, and stacked the Strehl-weighted significance maps of each frame in order to compute the final significance map for potential detections around LP 791-18. We measured our detection limits from the distribution of confidence levels among all apertures in a series of 5 pixel annuli around the primary. No apertures contain a statistically significant excess of flux within the NIRC2 field of view, and hence there are no detected astrophysical sources. We pursued similar analysis for both calibrators and found that they also have no astrophysical sources within the observed field of view (FOV).

The non-redundant masking observations use a pupil plane mask to resample the telescope into a sparse interferometric array. This allows the use of the complex triple product, or closure-phase observable, to remove non-common path errors produced by atmospheric conditions or variable optical aberrations. To remove systematics in the closure-phase observable, the observation of LP 791-18 was paired with observations of the two calibrator stars, both of which have similar color and brightness and are located within 1° of LP 791-18. Our analysis followed the methods described in the appendix of Kraus et al. (2008). Binary-source models were fit to the calibrated closure phases to search for significant evidence of binarity, and the detection limits were calibrated by repeatedly scrambling the phase errors and determining the distribution of binary fits. Again, no sources were detected in the masking data for LP 791-18.

Figure 5 shows the effective contrast achieved by our NIRC2 observations. The combination of aperture masking and imaging data excludes many companions to LP 791-18, reaching contrast ratios of $\Delta K' = 3.56$ mag at $\rho = 20$ mas, $\Delta K' = 4.67$ mag at $\rho = 40$ mas, $\Delta K' = 5.5$ mag at $\rho = 150$ mas, $\Delta K' = 6.6$ mag at $\rho = 200$ mas, and an ultimate limiting magnitude of $\Delta K' = 9.3$ mag at $\rho > 1''$. Comparison to the MIST isochrones (Morton 2015; Dotter 2016) for all

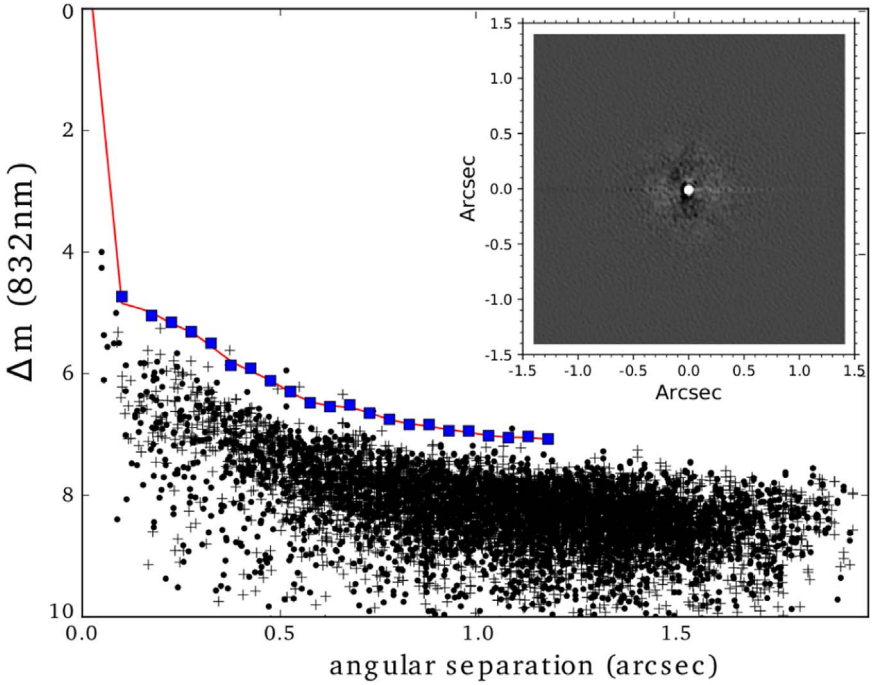

Figure 4. Red-optical contrast limits set by our Gemini/'Alopeke speckle imaging data, with the reconstructed image shown at inset. No secondary sources are detected.

stars at the same distance and with ages >100 Myr shows that our suite of high-resolution imaging data rule out all companions down to the H-burning limit from the NRM inner limit of 20 mas (0.8 au) out to the edge of the NIRC2 FOV in the dithered data set (9″, 230 au). We rule out all companions with spectral types >L5 beyond 1.1 au, >T4 beyond 5.4 au, and >T8 beyond 22 au (Dupuy & Liu 2012, 2017).

3. Ground-based Transit Photometry

3.1. Las Cumbres Observatory

We also observed both transit signals using 1.0 m telescopes of the Las Cumbres Observatory (LCO; Brown et al. 2013). We used the `TESS Transit Finder`, a customized version of the `Tapir` software package (Jensen 2013), to schedule the photometric follow-up observations. All observations used a 4096^2 LCO SINISTRO camera with an image scale of 0.″389 pixel^{-1} resulting in a 26′ × 26′ field of view.

We acquired one transit light curve of TOI-736.01 on 2019 June 16 at the South Africa Astronomical Observatory, and two light curves of TOI-736.02 on 2019 June 11 from two telescopes at Siding Spring. The transit of TOI-736.01 comprised 114 images in Bessel-I band using 60 s exposures, for a total duration of 169 minutes. The two transits of TOI-736.02 included 99 minutes in I_C band with 60 s exposures, and 192 minutes in Sloan i' with 100 s exposures. The target star had an average FWHM of 2.″2, 2.″4, and 1.″4, respectively. The nearest known *Gaia* DR2 star is 15″ from LP 791-18: it has $\Delta G_{\rm RP} = 4.3$ and so is too faint to significantly dilute the *TESS* transit photometry, (and our high-resolution imaging detected no additional companions), so the LCO follow-up apertures are negligibly contaminated by neighboring stars.

All data were calibrated by LCO's standard BANZAI pipeline and the photometric data were extracted using `AstroImageJ` (Collins et al. 2017). In all cases, the target starlight curve shows a clear transit detection, while a search for eclipsing binaries within 2.′5 that could have caused the transit signal reveals nothing. The transit signal can be reliably detected with apertures having radii as small as 1.″95, but systematic effects start to dominate for smaller apertures. Figure 6 shows our LCO photometry, in which transits are clearly visible.

We model all three LCO light curves with `BATMAN` (Kreidberg 2015) keeping all parameters—except for R_p/R_* and the mid-transit time—fixed to the values derived from the *TESS* light curve (Table 2). We also include a linear airmass correction model to account for the out-of-transit baseline, and limb darkening was calculated using `LDTK` (Parviainen & Aigrain 2015) based on the parameters in Table 1. For TOI-761.01 we measure $T_0 = 2458651.29807 \pm 0.00041$ and $R_p/R_* = 0.1233 \pm 0.0024$ (a 51σ detection), while for TOI-761.02 we measure $T_0 = 2458645.94429 \pm 0.00078$ and $R_p/R_* = 0.0624 \pm 0.0044$ (a 14σ detection). The LCO transit depths are all consistent with those measured by *TESS*.

3.2. MEarth-South

LP 791-18 is also a target of the MEarth transit survey (Nutzman & Charbonneau 2008; Irwin et al. 2015). The MEarth data set consists of 4534 photometric observations obtained with the MEarth-South telescope array between 2015 May and 2019 June. These photometric data do not reveal any coherent periodic variations that would indicate a stellar rotation period.

A box-least squares (BLS) search of the MEarth photometry independently reveals a signal with a period of 0.948002 day (shown in Figure 6), which is consistent with the TESS ephemeris of TOI-736.02. The detection significance using MEarth data alone is 9σ, and is substantially lower when not including the data from the latest MEarth observational season, which is why this planet was not previously identified by the MEarth team. Due to the near-integer orbital period of TOI-

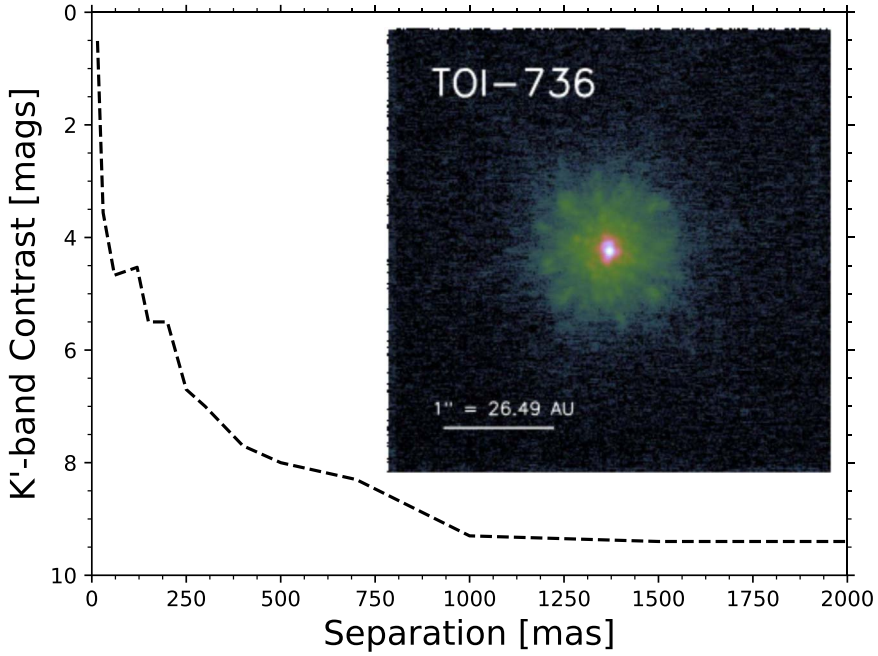

Figure 5. K'-band contrast limits set by our Keck/NIRC2 AO imaging and aperture masking data, with the imaging data shown at inset. No secondary sources are detected.

736.01, its transits cannot be recovered in the MEarth photometry (though some combinations of P and T_0 are ruled out).

We used `BATMAN` and `emcee` to model the transits of TOI-736.02 using the combined TESS and MEarth photometry. The values of a/R_* and i were kept fixed at the values obtained from the TESS analysis (Table 2) while T_0, P, and R_p/R_* were allowed to vary. From this analysis we measure $T_0 = 2458645.9434 \pm 0.0013$, $P = 0.9480048 \pm 0.0000058$ day, and $R_P/R_* = 0.059^{+0.0033}_{-0.0042}$ (a detection significance of 15σ).

3.3. Refined Transit Parameters

We use the LCO and MEarth-South data sets to improve the ephemerides and transit depths of both transit signals by taking the weighted mean of R_P/R_* and combining the T_0 values using weighted least squares and assuming a linear ephemeris. For TOI-736.01 (undetected by MEarth) we use the results of the *TESS* and LCO transit analyses, while for TOI-736.02 we use the results of the LCO transit and the combined *TESS*+MEarth analysis.

We find that for each signal, R_P/R_* is consistent across all our analyses and T_0 is consistent with a linear ephemeris. Including the ground-based data decreases the uncertainty on P by an order of magnitude (for TOI-736.01) and two orders of magnitude (for TOI-736.02). We report the final values of R_P/R_*, R_P, T_0, and P for both TOIs in Table 2.

4. Statistical Validation of the Candidates

Although transits are clearly seen by *TESS* (Figure 1) and from the ground (Figure 6), many *TESS* candidates have been identified as false positives[40] and so we must verify that the observed signals are planetary in origin. Because the precise Doppler spectroscopy needed to confirm these signals as planets will likely need to wait until LP 791-18 rises again for the next season, we demonstrate below that the signals are far more likely to be planetary than of any other origin. Below, we consider whether LP 791-18 could be blended with a background eclipsing binary, and then whether LP 791-18 itself could be a multiple star system. We find that both scenarios are unlikely, indicating that our planet candidates are likely to be true transiting planets.

4.1. Independent Signal Validation

We used the Discovery and Validation of Exoplanets tool[41] (`dave`; Kostov et al. 2019a, 2019b), along with the short-cadence pixel files and photometry, to independently estimate the quality of the candidate planet signals. We find no significant secondary eclipses or odd–even differences (which would otherwise indicate an eclipsing binary instead of a transiting planet) for either TOI. We find no significant photocenter shift (which would indicate a blend of multiple stars, and possible source confusion) for TOI-736.01. For TOI-736.02 the individual difference images per transit are too noisy for `dave` to provide an accurate photocenter analysis. Nonetheless, neither candidate shows indications of being a false positive.

The `dave` results are consistent with the *TESS* project's data validation tests (Twicken et al. 2018; Li et al. 2019), which both TOIs passed. These tests include the odd–even transit depth test, the weak secondary test, the ghost diagnostic test, the difference image centroid offset test (0.35 and 0.5sigma for the TIC offset for candidates 1 and 2, respectively, representing less than $1''$ offsets from the TIC position), and the statistical bootstrap test (which gave 7×10^{-73} and 3×10^{-15} for TOIs 736.01 and .02, respectively).

4.2. Unassociated Background Scenarios

Our ground-based photometry demonstrates that transits occur close to LP 791-18, but a background system could lie

[40] https://exofop.ipac.caltech.edu/tess/

[41] https://github.com/barentsen/dave

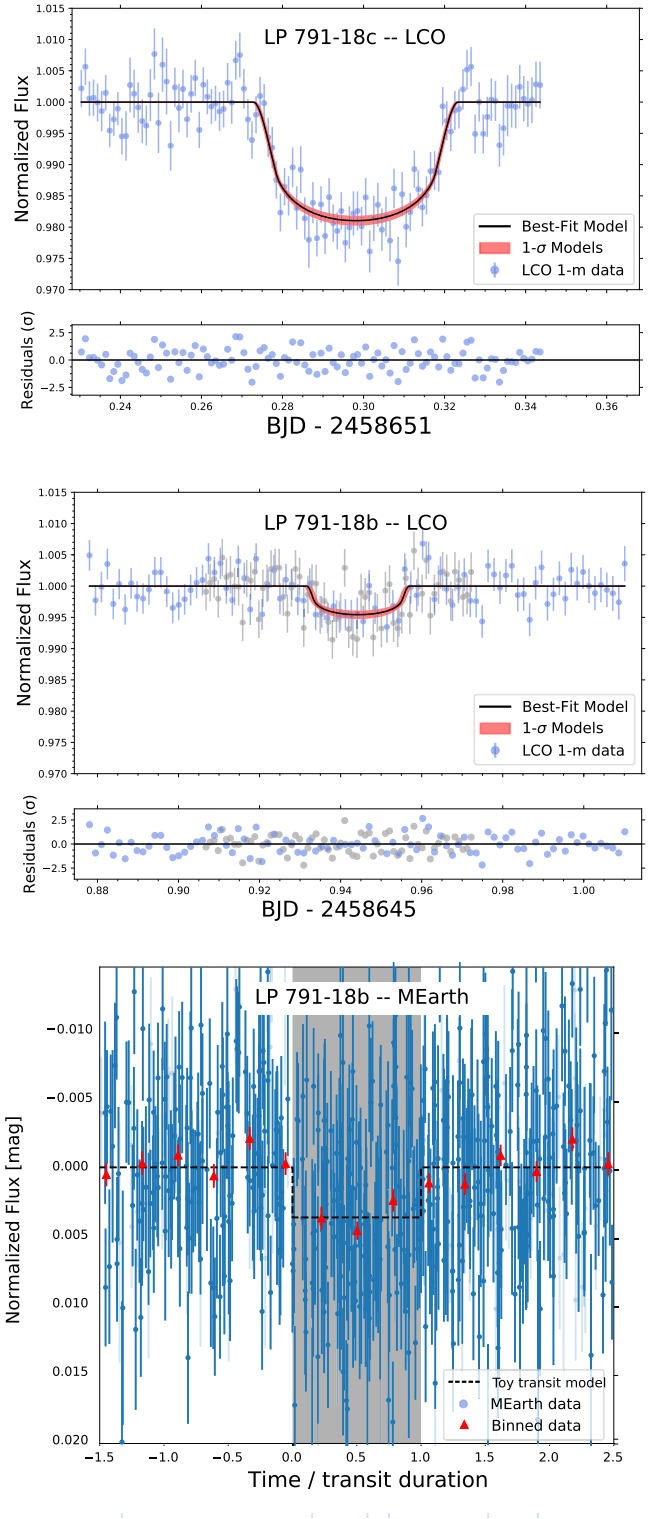

Figure 6. Ground-based photometry of LP 791-18. Top: one LCO 1 m transit of LP 791-18c. Middle: two LCO 1 m transits of LP 791-18b. Bottom: phase-folded MEarth-South photometry of LP 791-18b during transit.

near the star and mimic planetary transits. Given its high proper motion, LP 791-18 has moved considerably since its detection by the Palomar Optical Sky Survey (POSS) in the 1950s. No source is visible in the digital POSS-I images at the star's location during the *TESS* epoch. By comparing these images to SDSS ninth data release (DR9) photometry, we confidently exclude any background object down to a limit of approximately $r = 19.5$, $i = 18.6$ (AB mags), corresponding to $R \approx 19.2$, $I_C \approx 18.3$ (Vega mags[42]). Because the broad *TESS* bandpass is quite red (Ricker et al. 2014), we assume that the limiting *TESS* magnitude is $T \approx I_C \approx 18.3$, 4.8 mag fainter than LP 791-18. We therefore exclude all background sources as the source of TOI-736.01's transits.

From POSS-I and *TESS* alone we cannot rule out all such background scenarios for the shallower TOI-736.02 (as its transit depth is $<10^{-0.4 \times 4.8}$), but our LCO transit observations demonstrate that these events occur within a few arcsec of LP 791-18. Because our high-resolution imaging shows no additional sources, this all but eliminates the chance that this shallower candidate is a background system. A 4.8 mag fainter source could reproduce the 736.02 transits (with depth roughly 0.4%) if it had a 40% (intrinsic) transit depth—or if it had $T \approx 19.4$ mag and were completely eclipsed. The only allowable brightness of a background source is T in the range 18.3–19.4 mag. We used the TRILEGAL Galactic stellar population simulator[43] (Girardi et al. 2005) to find a 0.2% chance that our LCO photometric aperture would contain a star with this brightness. If these simulated stars were actually equal-mass binaries with $P = 0.95$ day, then the average transit probability of the ensemble (assuming $e = 0$) is 17%. The median star in this distribution is a $0.4\,M_\odot$ M dwarf, and the tight binary fraction of such stars is about 3% (Blake et al. 2010; Clark et al. 2012). The product of these factors is the likelihood that TOI-736.02 is a background false positive: this is 10^{-5}, so we conclude that both transit signals are unlikely to arise from blends with a background eclipsing binary.

4.3. Bound, Multi-star Scenario

We now consider the scenario that LP 791-18 is itself a multiple system with transits occurring around just one component—this, too, turns out to be unlikely. M dwarfs in the Solar neighborhood with 0.075–0.3 $M_\odot$ have a multiplicity fraction of about 20% (Winters et al. 2019). Following the parameters given in that work, we simulated a distribution of binary companions to LP 791-18 with a log-normal distribution in a that peaks at 10 au, with $\sigma_{\log_{10}(a/\mathrm{au})} = 1$, and with a linearly increasing mass fraction distribution from 0.1 to unity.

We then compare this population of plausible companions to our observations: we see no companions in our high-resolution imaging; the system is not overluminous relative to the M dwarf H-R diagram; the host star's density is constrained by the transit light-curve analysis ($\rho_{*,\mathrm{circ}}$ in Table 2; Seager & Mallén-Ornelas 2003); companions of later type than roughly L5 ($M \lesssim 0.03\,M_\odot$) would be too faint to be the source of the transit signals (Dahn et al. 2002); and we see no evidence for secondary lines in our high-resolution optical spectrum. Figure 7 shows that our observations cover all relevant regions of false positive parameter space.

After accounting for the possibility that, by chance, some wide companions could have a very low projected separation from LP 791-18 and some short-period companions could have had zero velocity offset from LP 791-18, we still find just a 0.7% chance that an additional companion is the source of the transit signals and went unnoticed by our observations. The remaining possible configurations involve a 0.03–0.04 $M_\odot$

[42] http://www.sdss3.org/dr8/algorithms/sdssUBVRITransform.php
[43] http://stev.oapd.inaf.it/cgi-bin/trilegal

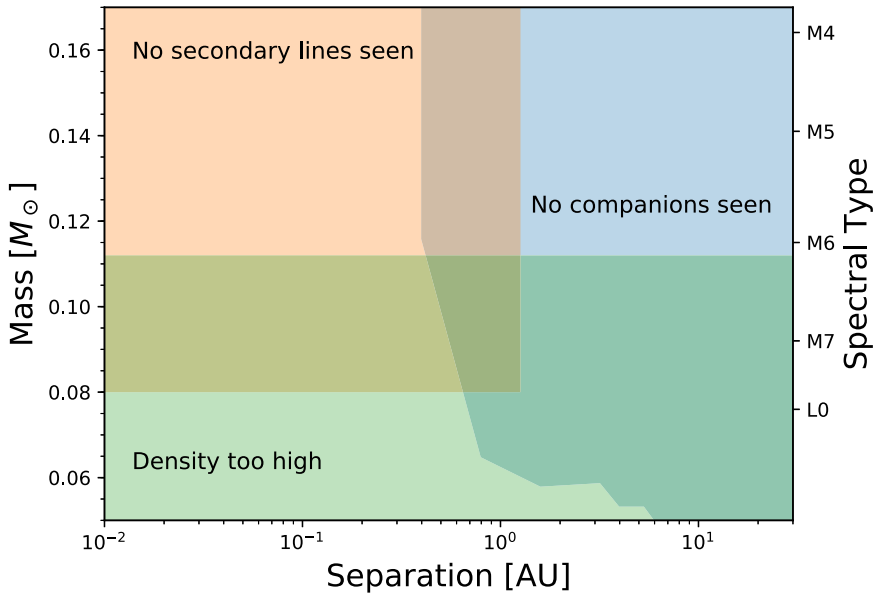

Figure 7. Our analysis rules out bound companions of all types as the hosts of the detected transits. Clockwise from upper left: we see no secondary lines in our high-resolution spectra, ruling out bright, short-period companions; we see no companions in our high-resolution imaging data, ruling out long-period companions; and our transit analysis indicates a density than excludes objects with $<0.11\ M_\odot$. See Section 4.3 for details.

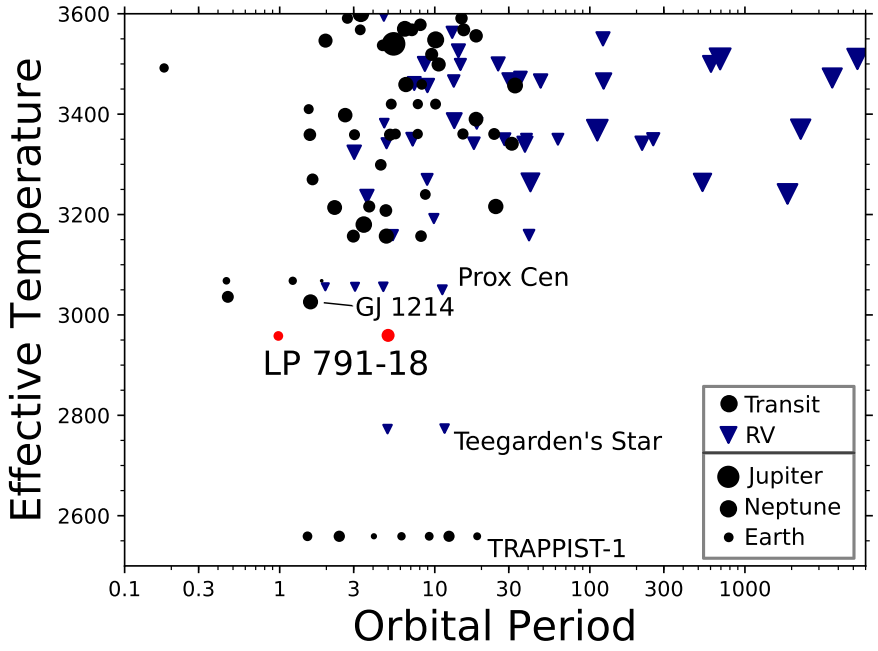

Figure 8. Planets orbiting cool dwarfs. The point size increases as the logarithm of planet mass (inferred from radius when the mass are unknown). Transiting planets are shown with circles and planets not known to transit with triangles; our two new planets are indicated by red circles.

brown dwarf orbiting LP 791-18 with $a \approx 0.7$ au and nearly or fully eclipsed by a giant planet or brown dwarf.

Taking the distribution of mass fractions and semimajor axes of low-mass stellar binaries (Winters et al. 2019), and accounting for random orbital alignments, we calculate that a star like LP 791-18 has a 0.04% chance of being in an eclipsing binary with $P \leqslant 10$ days and companion mass 0.03–0.04 $M_\odot$. This is far less than its 66% chance of having a planet with with $R_P < 3R_\oplus$ on a similar period (Dressing & Charbonneau 2015). It is therefore far more likely that LP 791-18 is a single planet-hosting star than that it is a false positive with a eclipsing brown-dwarf binary. Thus we conclude that the signals detected by *TESS* represent exoplanets transiting the M6V star LP 791-18. Henceforth, we denote TOI-736.02 (the smaller, inner planet) as LP 791-18b and TOI-736.01 as LP 791-18c.

5. Discussion

5.1. On Multiplicity and Additional Planets

There is evidence that the multiplicity of short-period planets is high for stars at the latest spectral types, even though few planet host stars are known at these coolest temperatures (see Figure 8). Aside from LP 791-18, just seven planetary systems are known with $T_{\rm eff} < 3100$ K. Four of these are multiple systems: TRAPPIST-1 (seven planets; Gillon et al. 2016, 2017), YZ Ceti (three planets; Astudillo-Defru et al. 2017;

Robertson 2018), Kepler-42 (three planets; Muirhead et al. 2012), and Teegarden's Star (two planets; Zechmeister et al. 2019). Three have just a single known planet: GJ 1214 (Charbonneau et al. 2009), LHS 3844 (Vanderspek et al. 2019), and Proxima Centauri (Anglada-Escudé et al. 2016).

To verify that additional planets could exist on stable orbits around LP 791-18 with P between the two transiting planets, we performed a series of N-body dynamical simulations using the Mercury Integrator Package (Chambers 1999) and following the methodology of Kane (2015). We assessed the stability of circular orbits between the two known planets by placing a hypothetical Earth-mass planet at a in the range 0.01–0.03 au in steps of 0.0005 au. Each simulation was run for 10^5 yr, a sufficient time span given the very short orbital periods involved. Our simulations show that stable orbits are possible in the range 0.011–0.0255 au (although large planets close to low-order resonance with LP 791-18c are unlikely due to the absence of observed TTVs).

To look for additional planets, we ran a BLS analysis of the *TESS* photometry but found no significant signals. We also injected a series of planet transit signals into the *TESS* photometry and ran a BLS analysis on the simulated data. For an intermediate period (e.g., 2.5 days), transiting planets with $R_P \gtrsim 1.2R_\oplus$ should have been seen in the *TESS* data. For planets on longer periods (e.g., $P = 7$–10 days), $R_P \gtrsim 1.4R_\oplus$ would have been detected. Thus, planets the size of those orbiting TRAPPIST-1 would be unlikely to have been detected by *TESS* around LP 791-18. There could easily be Earth-sized planets orbiting LP 791-18 that went undetected by *TESS*. In particular, the cloud-free habitable zone for a star like LP 791-18 extends from approximately $P = 10$–30 days (Kopparapu et al. 2013, 2014), a range only poorly sampled by the existing *TESS* photometry.

Additional planets could be identified by long-duration time-series photometry (as were sought around GJ 1214; Fraine et al. 2013; Gillon et al. 2014, and seen around TRAPPIST-1; Gillon et al.; Luger et al.). However, just a few degrees of mutual misalignment between the planets' orbits would result in any extra planets failing to transit. Assuming circular orbits, Earth-size planets with $P = 2.5$ days and 7 days would need to be misaligned by $2\overset{\circ}{.}7$ and $1\overset{\circ}{.}3$, respectively, in order not to transit. For reference, the mutual misalignments of the TRAPPIST-1 planets are $<0\overset{\circ}{.}4$ (Gillon et al. 2017), while many other ultra-short-period planets have much higher mutual inclinations of $6\overset{\circ}{.}7$ (Dai et al. 2018).

5.2. LP 791-18b and c

These two small planets have sizes of $1.1R_\oplus$ and $2.3R_\oplus$, and so straddle the radius gap at about $1.8R_\oplus$ that separates smaller, higher-density super-Earths from larger, more rarified sub-Neptunes (Fulton et al. 2017; Fulton & Petigura 2018). It remains an open question as to whether this radius gap (measured from FGK systems) extends to planets orbiting M dwarfs, or to planets with this combination of small size and low irradiation.

It seems entirely likely that the masses of these new planets can be measured in the near future, which would help to better determine their overall composition. By comparison to theoretical mass–radius relations (Valencia 2011) we expect the two planets to have masses of 0.5–4$M_\oplus$ (for bulk compositions ranging from Moon-like to Mercury-like) and 5–20$M_\oplus$ (for bulk compositions ranging from a 50–50 water-rock mix to a 0.01% H_2/He veneer on a rocky core) for planets b and c, respectively. These compositions correspond to RV semi-amplitudes of 1–9 and 7–26 m s^{-1}. A mass and radius could distinguish between different refractory compositions of LP 791-18b, but the degeneracies inherent in modeling larger planets means that RV observations can constrain, but not uniquely determine, the bulk makeup of LP 791-18c. The star's red color and relatively low apparent brightness means that RV follow-up is likely to be most productive when pursued by facilities on large ($\geqslant$8 m) telescopes and/or with extended coverage into the red-optical or near-infrared.

Because of the poor constraints on the impact parameters in the light curve, we cannot deduce much about the mutual inclination of these two planets; measurement of the Rossiter-McLaughlin effect or Doppler tomography observations would provide an orthogonal constraint on the dynamical architecture. However, these measurements are probably only feasible if LP 791-18 has $v \sin i \gtrsim 2$ km s^{-1}, which is substantially larger than expected for a quiescent star of this type (though barely consistent with our Keck/HIRES and Subaru/IRD spectra). Even then, the short transit durations would make it difficult to obtain the necessary S/N in exposures that are short enough to provide good temporal sampling of the transit.

Atmospheric characterization of these planets is also feasible. We simulated model transmission spectra for these planets using `ExoTransmit` (Kempton et al. 2017) and assuming planet masses of 2$M_\oplus$ and 7$M_\oplus$, and atmospheric compositions of 100% H_2O and 100× Solar metallicity, for LP 791-18b and c, respectively. Our model atmospheres assumed no clouds and chemical equilibrium, and set the 1 bar radius equal to the transit radius observed by *TESS*. These models predict peak-to-valley transmission signals for planets b and c of roughly 150 and 500 ppm, with the difference set largely by the two models' differing mean molecular weights. If the planets have lower masses or lower-metallicity atmospheres than assumed above the desired atmospheric signals would be even stronger, though in the presence of clouds the signals would be weaker.

We then used PandExo[44] (Greene et al. 2016; Batalha et al. 2017) to simulate *James Webb Space Telescope* (*JWST*) observations of a single transit of each planet using the NIRspec prism (0.6–5 μm) and MIRI LRS (5–12 μm) instruments modes, with a baseline of equal time to the transit time and zero noise floor. Assuming an effective resolution of 35 we find that the median per-channel uncertainty on the transit depth would be 220 ppm and 150 ppm, respectively, with the difference set by the planets' transit durations. For the larger, cooler LP 791-18c *JWST* could identify atmospheric features in the spectrum between 1 and 5 μm with just a single transit, indicating that it could be a compelling target for atmospheric follow up. For the smaller, warmer LP 791-18b multiple transits would likely be needed to probe the composition of the planet's atmosphere (if any).

5.3. Concluding Thoughts

Figure 8 shows that LP 791-18 is the third-coolest star known to host planets. The discovery of the TRAPPIST-1 system spurred many new studies into star-planet interactions (Dong et al. 2018), multiplanet dynamics (Luger et al. 2017), atmospheric escape (Wang & Dai 2018), planet formation

[44] https://github.com/natashabatalha/PandExo

(Haworth et al. 2018), and atmospheric measurements (Barstow & Irwin 2016) of small planets around low-mass stars. Along with the new planets orbiting Teegarden's Star (Zechmeister et al. 2019), LP 791-18 now adds another multiplanet system against which to test these theories via the system properties presented here, through further detailed characterization of the planets and their host star, and by searching for additional planets orbiting this cool dwarf.

The authors thank our anonymous referee for constructive comments that improved the quality of this work. We also thank Prof. N. Lewis for a stimulating and thought-provoking discussion that improved the quality of this work. We thank Hiroki Harakawa, Tomoyuki Kudo, Masashi Omiya, Aoi Takahashi, the entire IRD team, and the Subaru IRD TESS intensive follow-up project team for supporting Subaru IRD observation.

I.J.M.C. acknowledges support from the NSF through grant AST-1824644, and from NASA through Caltech/JPL grant RSA-1610091. M.R.K. acknowledges support from the NSF Graduate Research Fellowship, grant No. DGE 1339067. D.H. acknowledges support by the National Aeronautics and Space Administration (80NSSC18K1585, 80NSSC19K0379) awarded through the *TESS* Guest Investigator Program. Work by J.N.W. was supported by the Heising-Simons Foundation. B.R-A. acknowledges support from FONDECYT through grant 11181295. W.W. acknowledges support from the NSF GRFP, DGE 1650115. N.N. is supported by JSPS KAKENHI grant Nos. JP18H01265 and JP18H05439, and JST PRESTO grant No. JPMJPR1775. A.J.C. acknowledges support from the National Science Foundation Graduate Research Fellowship Program under grant No. DGE 1842402. D.B. acknowledges support from an NSERC PGS-D scholarship. D.D. acknowledges support provided by NASA through Hubble Fellowship grant *HST*-HF2-51372.001-A awarded by the Space Telescope Science Institute, which is operated by the Association of Universities for Research in Astronomy, Inc., for NASA, under contract NAS5-26555. The MEarth Team gratefully acknowledges funding from the David and Lucille Packard Fellowship for Science and Engineering (awarded to D.C.) and the National Science Foundation under grants AST-0807690, AST-1109468, AST-1004488 (Alan T. Waterman Award), and AST-1616624. This publication was made possible through the support of a grant from the John Templeton Foundation. The opinions expressed in this publication are those of the authors and do not necessarily reflect the views of the John Templeton Foundation.

We acknowledge the use of *TESS* Alert data, which is currently in a beta test phase, from pipelines at the *TESS* Science Office and at the *TESS* Science Processing Operations Center. This research has made use of the Exoplanet Follow-up Observation Program website, which is operated by the California Institute of Technology, under contract with the National Aeronautics and Space Administration under the Exoplanet Exploration Program. This Letter includes data collected by the *TESS* mission, which are publicly available from the Multimission Archive for Space Telescopes (MAST). Some of the observations in this Letter made use of the High-Resolution Imaging instrument 'Alopeke at Gemini-North. 'Alopeke was funded by the NASA Exoplanet Exploration Program and built at the NASA Ames Research Center by Steve B. Howell, Nic Scott, Elliott P. Horch, and Emmett Quigley. Resources supporting this work were provided by the NASA High-End Computing (HEC) Program through the NASA Advanced Supercomputing (NAS) Division at Ames Research Center for the production of the SPOC data products. The authors wish to recognize and acknowledge the very significant cultural role and reverence that the summit of Maunakea has always had within the indigenous Hawaiian community. We are most fortunate to have the opportunity to conduct observations from this mountain.

Data and materials availability: All associated data products are available for download from ExoFOP-*TESS* website, https://exofop.ipac.caltech.edu/tess/target.php?id=181804752.

Facilities: TESS, *Gaia*, Gemini ('Alopeke), Keck I (HIRES), Keck II (NIRC2), Subaru (IRD), LCO.

ORCID iDs

William Waalkes https://orcid.org/0000-0002-8961-0352
Elisabeth R. Newton https://orcid.org/0000-0003-4150-841X
Norio Narita https://orcid.org/0000-0001-8511-2981
Philip Muirhead https://orcid.org/0000-0002-0638-8822
Kristo Ment https://orcid.org/0000-0001-5847-9147
Adam Kraus https://orcid.org/0000-0001-9811-568X
Veselin Kostov https://orcid.org/0000-0001-9786-1031
Molly R. Kosiarek https://orcid.org/0000-0002-6115-4359
Stephen R. Kane https://orcid.org/0000-0002-7084-0529
Howard Isaacson https://orcid.org/0000-0002-0531-1073
Sam Halverson https://orcid.org/0000-0003-1312-9391
Mark Everett https://orcid.org/0000-0002-0885-7215
Diana Dragomir https://orcid.org/0000-0003-2313-467X
Karen A. Collins https://orcid.org/0000-0001-6588-9574
Ashley Chontos https://orcid.org/0000-0003-1125-2564
David Berardo https://orcid.org/0000-0001-6298-412X
Joshua N. Winn https://orcid.org/0000-0002-4265-047X
Nicholas J. Scott https://orcid.org/0000-0003-1038-9702
Aaron C. Rizzuto https://orcid.org/0000-0001-9982-1332
Erik A. Petigura https://orcid.org/0000-0003-0967-2893
Teo Mocnik https://orcid.org/0000-0003-4603-556X
Chelsea Huang https://orcid.org/0000-0003-0918-7484
Andrew W. Howard https://orcid.org/0000-0001-8638-0320
Trent Dupuy https://orcid.org/0000-0001-9823-1445
Courtney D. Dressing https://orcid.org/0000-0001-8189-0233
Paul A. Dalba https://orcid.org/0000-0002-4297-5506
David Charbonneau https://orcid.org/0000-0002-9003-484X
Jennifer Burt https://orcid.org/0000-0002-0040-6815
Joseph D. Twicken https://orcid.org/0000-0002-6778-7552
Motohide Tamura https://orcid.org/0000-0002-6510-0681
Joshua Schlieder https://orcid.org/0000-0001-5347-7062
David W. Latham https://orcid.org/0000-0001-9911-7388
Jon M. Jenkins https://orcid.org/0000-0002-4715-9460
Yasunori Hori https://orcid.org/0000-0003-4676-0251
Knicole Colon https://orcid.org/0000-0001-8020-7121

References

Albareti, F. D., Allende Prieto, C., Almeida, A., et al. 2017, ApJS, 233, 25
Anglada-Escudé, G., Amado, P. J., Barnes, J., et al. 2016, Natur, 536, 437
Astudillo-Defru, N., Díaz, R. F., Bonfils, X., et al. 2017, A&A, 605, L11
Bailer-Jones, C. A. L., Rybizki, J., Fouesneau, M., Mantelet, G., & Andrae, R. 2018, AJ, 156, 58
Barstow, J. K., & Irwin, P. G. J. 2016, MNRAS, 461, L92

Batalha, N. E., Kempton, E. M.-R., & Mbarek, R. 2017, ApJL, 836, L5
Benedict, G. F., Henry, T. J., Franz, O. G., et al. 2016, AJ, 152, 141
Berardo, D., Crossfield, I. J. M., Werner, M., et al. 2019, AJ, 157, 185
Blake, C. H., Charbonneau, D., & White, R. J. 2010, ApJ, 723, 684
Bonfils, X., Delfosse, X., Udry, S., et al. 2013, A&A, 549, A109
Brown, T. M., Baliber, N., Bianco, F. B., et al. 2013, PASP, 125, 1031
Chambers, J. E. 1999, MNRAS, 304, 793
Charbonneau, D., Berta, Z. K., Irwin, J., et al. 2009, Natur, 462, 891
Chontos, A., Huber, D., Latham, D. W., et al. 2019, AJ, 157, 192
Chubak, C., Marcy, G., Fischer, D. A., et al. 2012, arXiv:1207.6212
Claret, A. 2018, A&A, 618, A20
Clark, B. M., Blake, C. H., & Knapp, G. R. 2012, ApJ, 744, 119
Collins, K. A., Kielkopf, J. F., Stassun, K. G., & Hessman, F. V. 2017, AJ, 153, 77
Crossfield, I. J. M., Ciardi, D. R., Isaacson, H., et al. 2017, AJ, 153, 255
Crossfield, I. J. M., Ciardi, D. R., Petigura, E. A., et al. 2016, ApJS, 226, 7
Cutri, R. M., Wright, E. L., & Conrow, T. 2012, VizieR Online Data Catalog: WISE All-Sky Data Release
Dahn, C. C., Harris, H. C., Vrba, F. J., et al. 2002, AJ, 124, 1170
Dai, F., Masuda, K., & Winn, J. N. 2018, ApJL, 864, L38
Dong, C., Jin, M., Lingam, M., et al. 2018, PNAS, 115, 260
Dotter, A. 2016, ApJS, 222, 8
Dressing, C. D., & Charbonneau, D. 2013, ApJ, 767, 95
Dressing, C. D., & Charbonneau, D. 2015, ApJ, 807, 45
Dupuy, T. J., & Liu, M. C. 2012, ApJS, 201, 19
Dupuy, T. J., & Liu, M. C. 2017, ApJS, 231, 15
Fernandes, C. S., Van Grootel, V., Salmon, S. J. A. J., et al. 2019, ApJ, 879, 94
Foreman-Mackey, D., Hogg, D. W., Lang, D., & Goodman, J. 2013, PASP, 125, 306
Fraine, J., Deming, D., Gillon, M., et al. 2013, ApJ, 765, 127
Fulton, B. J., & Petigura, E. A. 2018, AJ, 156, 264
Fulton, B. J., Petigura, E. A., Howard, A. W., et al. 2017, AJ, 154, 109
Gagné, J., Mamajek, E. E., Malo, L., et al. 2018, ApJ, 856, 23
Gaia Collaboration, Brown, A. G. A., Vallenari, A., et al. 2018, A&A, 616 A1
Gillon, M., Demory, B.-O., Madhusudhan, N., et al. 2014, A&A, 563, A21
Gillon, M., Jehin, E., Lederer, S. M., et al. 2016, Natur, 533, 221
Gillon, M., Triaud, A. H. M. J., Demory, B.-O., et al. 2017, Natur, 542, 456
Girardi, L., Groenewegen, M. A. T., Hatziminaoglou, E., & da Costa, L. 2005, A&A, 436, 895
Greene, T. P., Line, M. R., Montero, C., et al. 2016, ApJ, 817, 17
Hardegree-Ullman, K. K., Cushing, M. C., Muirhead, P. S., & Christiansen, J. L. 2019, AJ, 158, 75
Haworth, T. J., Facchini, S., Clarke, C. J., & Mohanty, S. 2018, MNRAS, 475, 5460
Hayano, Y., Takami, H., Oya, S., et al. 2010, Proc. SPIE, 7736, 77360N
Howard, A. W., Johnson, J. A., Marcy, G. W., et al. 2010, ApJ, 721, 1467
Howard, A. W., Marcy, G. W., Bryson, S. T., et al. 2012, ApJS, 201, 15
Howell, S. B., Everett, M. E., Sherry, W., Horch, E., & Ciardi, D. R. 2011, AJ, 142, 19
Huang, C. X., Burt, J., Vanderburg, A., et al. 2018, ApJL, 868, L39
Ilin, E., Schmidt, S. J., Davenport, J. R. A., & Strassmeier, K. G. 2019, A&A, 622, A133
Irwin, J. M., Berta-Thompson, Z. K., Charbonneau, D., et al. 2015, in Conf. Proc. 18th Cambridge Workshop on Cool Stars, Stellar Systems, and the Sun, ed. G. van Belle & H. C. Harris (New York: Springer), 767
Jenkins, J. M. 2002, ApJ, 575, 493
Jenkins, J. M., Twicken, J. D., McCauliff, S., et al. 2016, Proc. SPIE, 9913, 99133E
Jenkins, J. S., Ramsey, L. W., Jones, H. R. A., et al. 2009, ApJ, 704, 975
Jensen, E. 2013, Tapir: A Web Interface for Transit/Eclipse Observability, version 2016, Astrophysics Source Code Library, ascl:1306.007
Kane, S. R. 2015, ApJL, 814, L9
Kempton, E. M.-R., Lupu, R., Owusu-Asare, A., Slough, P., & Cale, B. 2017, PASP, 129, 044402
Kerber, F., Nave, G., & Sansonetti, C. J. 2008, ApJS, 178, 374
Kesseli, A. Y., Kirkpatrick, J. D., Fajardo-Acosta, S. B., et al. 2019, AJ, 157, 63
Kiman, R., Schmidt, S. J., Angus, R., et al. 2019, AJ, 157, 231
Kolbl, R., Marcy, G. W., Isaacson, H., & Howard, A. W. 2015, AJ, 149, 18
Kopparapu, R. K., Ramirez, R., Kasting, J. F., et al. 2013, ApJ, 765, 131
Kopparapu, R. K., Ramirez, R. M., SchottelKotte, J., et al. 2014, ApJL, 787, L29
Kostov, V. B., Mullally, S. E., Quintana, E. V., et al. 2019a, AJ, 157, 124
Kostov, V. B., Schlieder, J. E., Barclay, T., et al. 2019b, AJ, 158, 32
Kotani, T., Tamura, M., Nishikawa, J., et al. 2018, Proc. SPIE, 10702, 1070211
Kraus, A. L., & Hillenbrand, L. A. 2007, AJ, 134, 2340
Kraus, A. L., Ireland, M. J., Huber, D., Mann, A. W., & Dupuy, T. J. 2016, AJ, 152, 8
Kraus, A. L., Ireland, M. J., Martinache, F., & Lloyd, J. P. 2008, ApJ, 679, 762
Kreidberg, L. 2015, PASP, 127, 1161
Li, J., Tenenbaum, P., Twicken, J. D., et al. 2019, PASP, 131, 024506
Luger, R., Sestovic, M., Kruse, E., et al. 2017, NatAs, 1, 0129
Luyten, W. J. 1979, New Luyten Catalogue of stars with proper motions larger than two tenths of an arcsecond; and first supplement; NLTT. (Minneapolis (1979)); Label 12 = short description; Label 13 = documentation by Warren; Label 14 = catalog
Mann, A. W., Dupuy, T., Kraus, A. L., et al. 2019, ApJ, 871, 63
Mann, A. W., Feiden, G. A., Gaidos, E., Boyajian, T., & von Braun, K. 2015, ApJ, 804, 64
Matson, R. A., Howell, S. B., Horch, E. P., & Everett, M. E. 2018, AJ, 156, 31
Morton, T. D. 2015, Isochrones: Stellar Model Grid Package, version 1.2.1, Astrophysics Source Code Library, ascl:1503.010
Morton, T. D., & Swift, J. 2014, ApJ, 791, 10
Muirhead, P. S., Dressing, C. D., Mann, A. W., et al. 2018, AJ, 155, 180
Muirhead, P. S., Johnson, J. A., Apps, K., et al. 2012, ApJ, 747, 144
Mulders, G. D., Pascucci, I., & Apai, D. 2015, ApJ, 814, 130
Newton, E. R., Irwin, J., Charbonneau, D., et al. 2016, ApJ, 821, 93
Newton, E. R., Irwin, J., Charbonneau, D., et al. 2017, ApJ, 834, 85
Newton, E. R., Mondrik, N., Irwin, J., Winters, J. G., & Charbonneau, D. 2018, AJ, 156, 217
Nutzman, P., & Charbonneau, D. 2008, PASP, 120, 317
Parviainen, H., & Aigrain, S. 2015, MNRAS, 453, 3821
Paudel, R. R., Gizis, J. E., Mullan, D. J., et al. 2019, MNRAS, 486, 1438
Pecaut, M. J., & Mamajek, E. E. 2013, ApJS, 208, 9
Reiners, A., & Basri, G. 2009, ApJ, 705, 1416
Ricker, G. R., Winn, J. N., Vanderspek, R., et al. 2014, Proc. SPIE, 9143, 20
Robertson, P. 2018, ApJL, 864, L28
Rojas-Ayala, B., Covey, K. R., Muirhead, P. S., & Lloyd, J. P. 2012, ApJ, 748, 93
Schlaufman, K. C., & Laughlin, G. 2010, A&A, 519, A105+
Scott, N. J., & Howell, S. B. 2018, Proc. SPIE, 10701, 107010G
Seager, S., & Mallén-Ornelas, G. 2003, ApJ, 585, 1038
Skrutskie, M. F., Cutri, R. M., Stiening, R., et al. 2006, AJ, 131, 1163
Smith, J. C., Stumpe, M. C., Van Cleve, J. E., et al. 2012, PASP, 124, 1000
Stassun, K. G., Corsaro, E., Pepper, J. A., & Gaudi, B. S. 2018a, AJ, 155, 22
Stassun, K. G., Oelkers, R. J., Pepper, J., et al. 2018b, AJ, 156, 102
Stumpe, M. C., Smith, J. C., Catanzarite, J. H., et al. 2014, PASP, 126, 100
Tuthill, P., Lloyd, J., Ireland, M., et al. 2006, Proc. SPIE, 6272, 62723A
Twicken, J. D., Catanzarite, J. H., Clarke, B. D., et al. 2018, PASP, 130, 064502
Valencia, D. 2011, in IAU Symp. 276, The Astrophysics of Planetary Systems: Formation, Structure, and Dynamical Evolution, ed. A. Sozzetti, M. G. Lattanzi, & A. P. Boss (Cambridge: Cambridge Univ. Press), 181
Vanderspek, R., Huang, C. X., Vanderburg, A., et al. 2019, ApJL, 871, L24
Vogt, S. S., Allen, S. L., Bigelow, B. C., et al. 1994, Proc. SPIE, 2198, 362
Wang, L., & Dai, F. 2018, ApJ, 860, 175
Winters, J. G., Henry, T. J., Jao, W.-C., et al. 2019, AJ, 157, 216
Wizinowich, P., Acton, D. S., Shelton, C., et al. 2000, PASP, 112, 315
Zechmeister, M., Dreizler, S., Ribas, I., et al. 2019, A&A, 627, A49